

**Research  
Article**

# Investigations of a Building-Integrated Ducted Wind Turbine Module

Robert K. W. Dannecker and Andrew D. Grant\*, Department of Mechanical Engineering, University of Strathclyde, Glasgow G1 1XJ, UK

**Key words:** renewable energy; wind turbine; ducting; built environment; CFD; wind tunnel; embedded generation

*So far, wind energy has not played a major role in the group of technologies for embedded generation in the built environment. However, the wind flow around conventional tall buildings generates differential pressures, which may cause an enhanced mass flow through a building-integrated turbine. As a first step, a prototype of a small-scale ducted wind turbine has been developed and tested, which seems to be feasible for integration into the leading roof edge of such a building. Here an experimental and numerical investigation of the flow through building-integrated ducting is presented. Pressure and wind speed measurements have been carried out on a wind tunnel model at different angles of incident wind, and different duct configurations have been tested. It was confirmed that wind speeds up to 30% higher than in the approaching freestream may be induced in the duct, and good performance was obtained for angles of incident wind up to  $\pm 60^\circ$ . The experimental work proceeded in parallel with computational fluid dynamics (CFD) modelling. The geometry of the system was difficult to represent to the required level of accuracy, and modelling was restricted to a few simple cases, for which the flow field in the building-integrated duct was compared with experimental results. Generally good agreement was obtained, indicating that CFD techniques could play a major role in the design process. Predicted power of the proposed device suggests that it will compare favourably with conventional small wind turbines and photovoltaics in an urban environment. Copyright © 2002 John Wiley & Sons, Ltd.*

## Introduction

The ducted wind turbine module is based on the principle of using the turbine casing to guide horizontal inflow to pass vertically through a turbine with a vertical shaft. A first device was patented in 1979 by a Glaswegian engineer.<sup>1</sup> It was intended for construction in modular form, either free-standing or as part of a larger structure. Evaluation and further refinement of the concept have been undertaken in the Department of Mechanical Engineering, University of Strathclyde,<sup>2</sup> and a first field trial at the National Wind Turbine Test Centre of the National Engineering Laboratory near Glasgow was encouraging.<sup>3</sup> In order to gain experience with the performance of the ducted wind turbine in the built environment, the latter prototype<sup>3</sup> was refurbished and mounted on the rooftop next to the Department's weather station (Figure 1). It features a high-solidity ( $\sigma = 0.73$ ) rotor of 480 mm diameter, and the shaft is directly connected to a Rutland 910 series generator (12 V single phase, rated 90 W). As with its predecessor, the prototype reached an electrical power coefficient (based on approaching wind velocity) in excess of 0.2 and tolerated between  $20^\circ$  and  $30^\circ$  of misalignment

\* Correspondence to: Andrew D. Grant, Department of Mechanical Engineering, University of Strathclyde, Glasgow G1 1XJ, UK. E-mail: agrant@mecheng.strath.ac.uk

Contract/grant sponsor: Marie Curie Research Fellowship, Commission of the European Communities, DG XII, Directorate-General for Science, Research and Development; Contract/grant number: JOR3-CT97-5008 (DG12-DEMA).

without significant loss of performance.<sup>4</sup> The turbine worked best at a tip speed ratio of around 1.5 and did not start at wind speeds lower than around  $5 \text{ m s}^{-1}$ .

In 1999, several prototypes of a hybrid photovoltaic–wind energy module (Figure 2) were manufactured in the Department’s workshop, with a rotor diameter of only 450 mm and solidity  $\sigma = 0.53$ . Each ducted wind turbine is rated at 90 W, with the integral photovoltaic spoiler at 85 W. Several of these devices have



*Figure 1. Free-standing prototype device on top of the James Weir Building, University of Strathclyde*

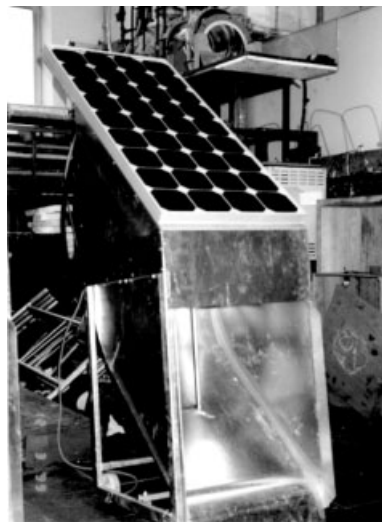


*Figure 2. Free-standing hybrid Photovoltaic–wind energy module prototype in the Department’s workshop, James Weir Building, University of Strathclyde*

been deployed on top of the ‘Lighthouse’ building in the inner city of Glasgow<sup>5</sup> to demonstrate the potential benefits of deploying renewable energy technologies in an urban environment.<sup>6</sup> So far, all the devices have been roof-mounted. They gain directly from the accelerated flow field around the leading edge.

In the present work,<sup>7,8</sup> completely integrated devices are proposed which are situated at the upper wall/roof edge (Figure 3). High wind speeds are induced in the duct owing to the pressure differential between the duct inlet at the front façade and the outlet at the flat roof. Wind approaching the building (Figure 4) generates a pressure distribution on the front façade, with highest positive pressures at 70%–90% of the building height. Air above this height flows upwards and that below flows downwards. At the sharp wall/roof edge the flow separates and local wind speed can exceed the mean flow velocity by a factor of two or more. Reattachment is possible should the roof be long enough. Significant suction occurs in the flow separation zone on the front part of the roof, and an edge vortex may develop, in particular for wind at an angle of incidence.

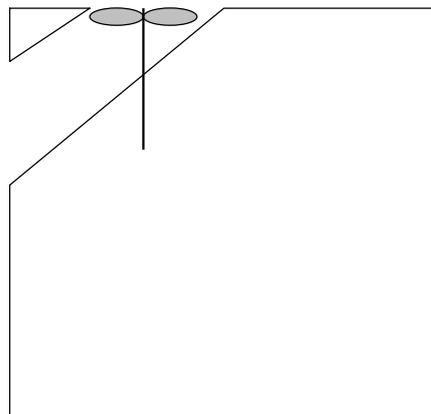


Figure 3. Ducted wind turbine integrated in the upper wall/roof edge, cross-sectional schematic sketch

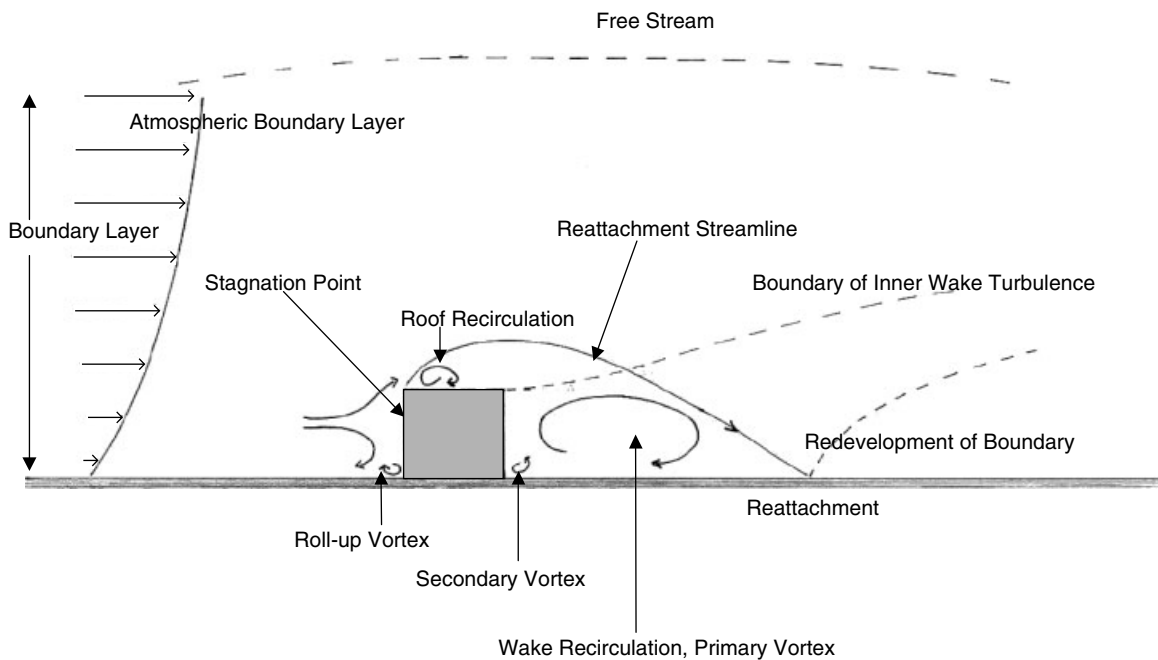


Figure 4. Mean flow streamline pattern for the flow around a building; schematic sketch

It is difficult to predict the flow through an integrated duct, in particular at different angles of incidence. The situation of flow entrainment at the duct outlet into a region where there is likely to be a generated edge vortex is very complex. The present work attempts to explore this complex flow problem by means of experimental and computational modelling.<sup>8</sup> The experiments were performed in the Department's open section low-speed wind tunnel, and the simulations were carried out with PHOENICS Version 2.2.1.<sup>9</sup>

## Experimental Modelling

### Experimental Set-up

A rectangular model building (up to 600 mm high, 350 mm wide and 200 mm deep) was constructed from Perspex and plywood. Its height could be adjusted by recessing it into a ground plane as shown in Figure 5, and its shape could be modified with different ducts and spoilers.<sup>10</sup> Pressure tapings, indicated by crosses in Figures 6–9, were located along the centreline of the front wall and on the roof, and in particular around the inlet, outlet and interior of each duct. The complete model/ground plane

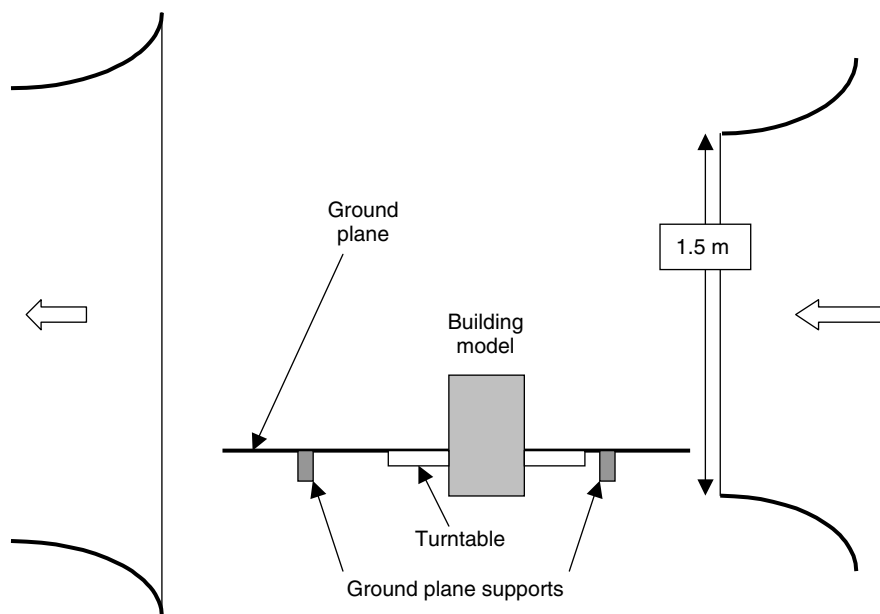


Figure 5. Schematic drawing of wind tunnel test configuration

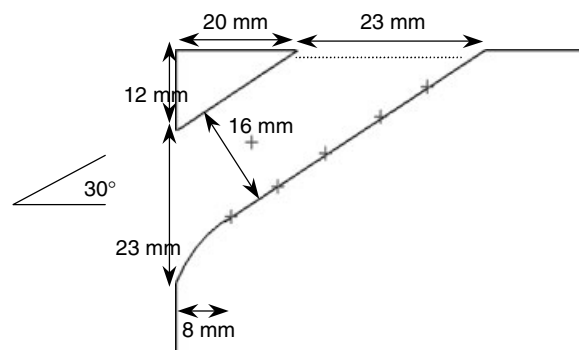


Figure 6. Cross-sectional view of 30° straight duct

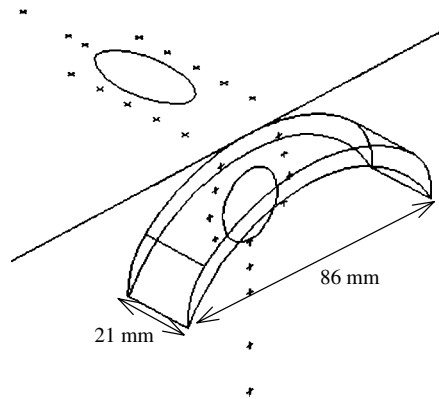


Figure 7. Three-dimensional view of 30° straight duct with wide spoiler at the inlet

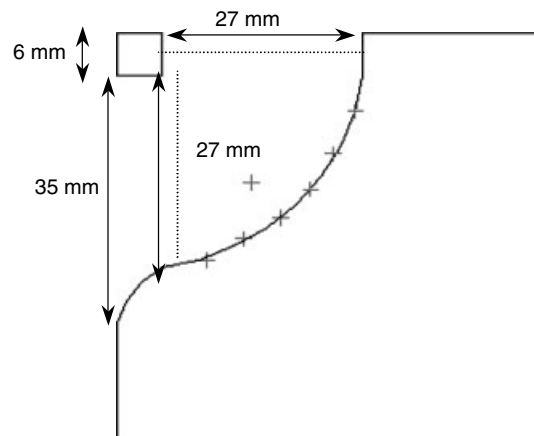


Figure 8. Cross-sectional view of 90° curved duct

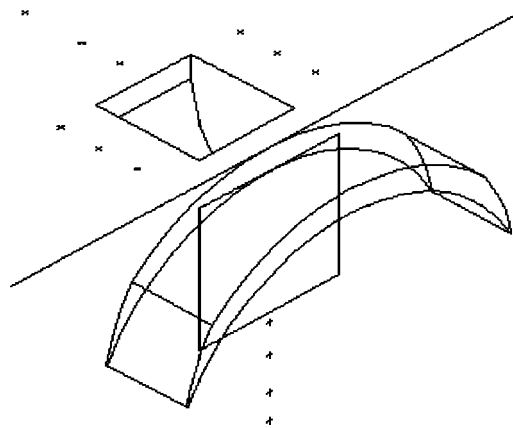


Figure 9. Three-dimensional view of 90° curved duct with wide spoiler at the inlet

assembly was then located in the open working section of the low-speed wind tunnel. In the ducts, along the symmetry line at inlet and outlet (dashed lines in Figures 6 and 8), local induced wind speeds were measured. A large number of different configurations were investigated; here, two of the most effective geometries, utilizing a wide spoiler at duct inlet, are presented. Tests on a simpler geometry

were used for comparison with the predictions from computational fluid dynamics, described in the next section.

The experiments were conducted at  $16.5 \text{ m s}^{-1}$  wind speed. Pressures obtained from the model's tappings were measured with an inclined manometer in parallel with a low-range ( $\pm 100 \text{ Pa}$ ) electromanometer with an accuracy of  $\pm 1.5 \text{ Pa}$ . Local velocities were obtained with a single hot wire constant temperature anemometer with a maximum error of less than 2%. The data acquisition system (LabVIEW) was set to a sampling frequency of 1 kHz and each recorded value was the average of 4096 samples.

The open section wind tunnel is of recirculating type, and the main flow deviates somewhat from the geometrical centreline of the working section, as will be evident from pressures on the front façade of the model building shown in Figure 10. With an empty working section, velocity is uniform (within 0.5%) and has a turbulence intensity below 1%. However, blockage effects are significant and in this study limited the maximum permissible height of the building model.

### Experimental Results for the Simple Building (without Duct)

To determine the areas of high pressure and suction, the model was first tested without a duct, and pressure values were recorded along the centreline of the front façade and the roof for different angles of oncoming wind. The steep decline of the pressure on the lower part of the building is due to a boundary layer created on the ground plane (Figure 10). Low peak values of  $C_p$  result from the finite width of the model and some small velocity shear in the wind tunnel free jet. The velocity profile (though not the turbulence structure) of the incoming flow is fairly representative of an urban environment. At full scale, of course, conditions would be dominated by the effect of upwind structures and so would vary greatly from site to site. The priority in these experiments was to create conditions over the upper region of the model which would permit comparative studies to be undertaken.

At the sharp edge between front façade and flat roof, suction occurs through flow separation (Figure 11). The uniform suction observed indicates that the whole roof is in the zone of separated flow. Larger angles of incidence cause higher suction at the upwind edge, and finally (at  $45^\circ$ ) the separating shear layer rolls up into the helix of vortex streets along both edges. A high pressure differential between the upper part of the front façade and the roof edge is thus maintained for angles of incidence of  $45^\circ$  or more. At these large angles a much lower suction ( $C_p = -0.2$ ) is seen downwind, indicating reattachment of the separated flow.

The present model develops pressure distributions which approximate to the standard results for a small-scale cube in the same range of Reynolds number.<sup>11</sup> Much higher values of suction ( $C_p = -1.15$ ) are reported for real-scale buildings at the front edge of the roof.<sup>12</sup>

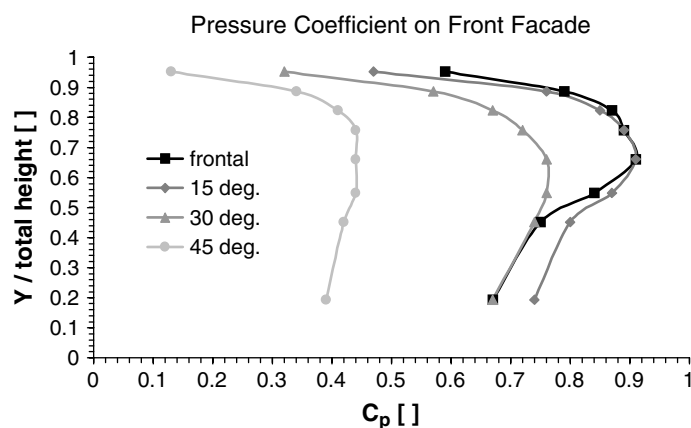


Figure 10. Pressure distribution along the centreline at the front façade for various angles of incidence

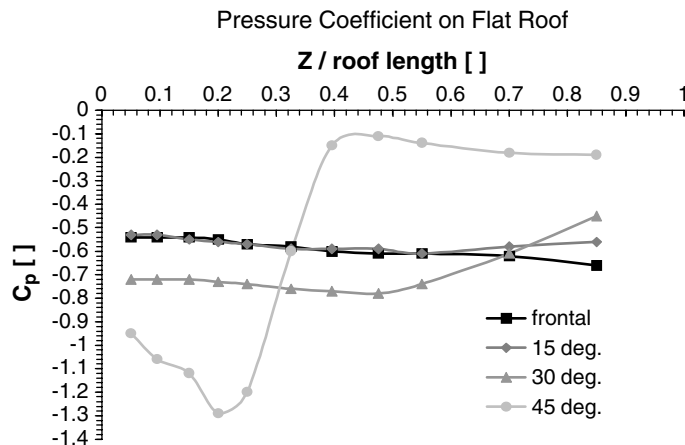


Figure 11. Pressure distribution along the centreline at the flat roof for various angles of incidence

**Experimental Results for the Building with Ducts and Spoiler**

With the 30° duct a spoiler on the front façade seems to act as a barrier to the upflow and directs the flow into the duct. At the duct exit, air speeds are recorded which are 35%–40% higher than the velocity of the approaching wind, with a fairly uniform velocity distribution along the centreline. This situation holds for angles of incidence up to 40° (Figure 12).

At larger angles of incidence the distribution becomes asymmetric as shown. The distribution of pressure in the duct indicates a swirling motion for larger angles of incidence. Over the front façade the situation is simpler. With larger angles of incidence the pressure decreases. Near the duct inlet the pressure on the leeward side is always higher than on the windward side. For a group of ducts mounted in a row, there seems unlikely to be any adverse interaction between adjacent duct entrances, for all wind approach angles. However, it may well be that the front wall will suffer a general drop in pressure when there are several ducts installed.

The impact of jet entrainment at the outlet on the surrounding pressure field is analysed by comparison of the average pressure coefficient differential between windward and leeward sides of the outlet. For each configuration of duct and attached spoiler the entrainment situation differs at larger angles of incidence. For the 30° duct the entrained jet disturbs the roof edge vortex and reduces the suction when carried downstream (Figure 13), but velocities similar to those measured for frontal incidence are still maintained. However, for

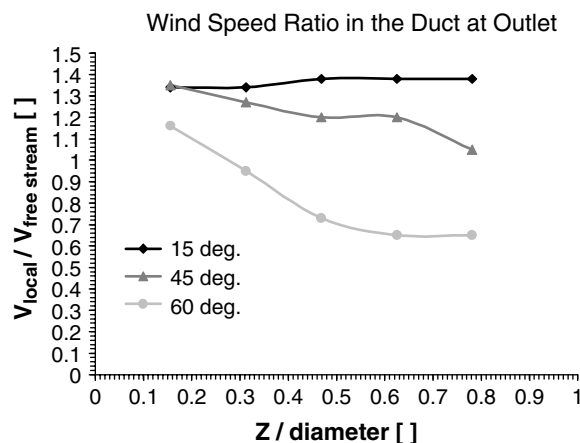


Figure 12. Induced high velocities in the 30° duct with front spoiler

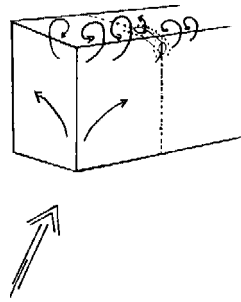


Figure 13. Duct flow entrainment into roof edge vortex; schematic sketch

the 90° curved duct, high velocities in the duct reinforce the vortex flow at the outlet. One might argue that the curved duct could interact beneficially with adjacent ducts along the roof edge.

Attaching the spoiler at the inlet of the 90° duct does not increase the inflow velocity, as was hoped. Indeed, it seems to promote flow separation in the lower part of the inlet, at least for larger angles of incidence (Figure 14). Maximum inflow occurs at 45° incident angle, and further rotation causes a decelerated flow field in the lower half of the duct inlet.

However, the wind velocity at outlet (Figure 15) has a peak value of over 40% above freestream velocity at 45°–65° incidence. The distribution drops smoothly towards the rear part of the outlet, corresponding with the lower inflow velocity in the lower part of the duct. For 65° incidence the configuration induces an average velocity which is still greater than the freestream. For each angle of incidence the outlet profile shows a significant drop in the upwind region. Better aerodynamic design of the upper edge of the duct could improve this flow situation.

### Summary of the Experimental Results and Conclusions

As the wind approaches the building model, it generates a high-pressure zone at the front façade and suction above the flat roof. These pressure zones communicate through an integrated duct at the wall roof edge. Both tested duct designs can induce a wind speed higher than that in the freestream, in the intended turbine plane at duct outlet. Spoilers above the inlet have been found to improve performance, giving higher wind speeds across the intended turbine plane while tolerating a wider range of incident wind direction. In order to compare the performance of different devices, the wind speed ratio (Figure 16) in

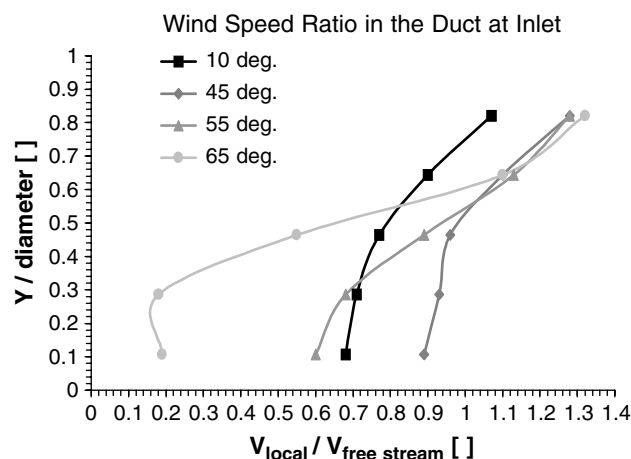


Figure 14. Inflow velocity of 90° duct with front spoiler for various angles of incidence

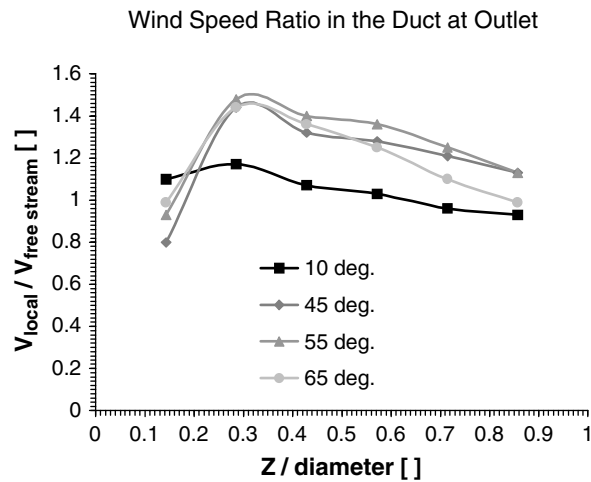


Figure 15. Induced high velocities in the 90° duct with front spoiler

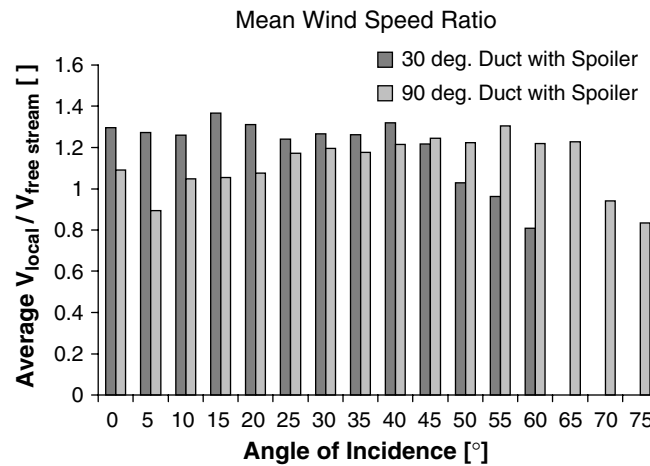


Figure 16. Mean wind speed ratio measured in the two duct configurations with spoiler for various angles of incidence

the duct outlet for each angle of incidence has been averaged. Each configuration reaches its best performance at a certain angle of incidence, and not for wind blowing normal to the façade. Exceeding the optimum angle leads to a drop in duct velocity below the freestream value. The velocity distribution in the duct becomes highly unsymmetrical, and it would be difficult to operate a turbine in this regime.

When there is an increased velocity in the outlet plane, the velocity distributions along the centreline are never uniform or completely symmetrical, but the measured profile should be acceptable to a turbine with soft stalling characteristics. Very encouraging is the wide range of tolerated angles of incidence, which exceeds the  $\pm 30^\circ$  observed for the first free-standing prototypes (see Introduction).

Wind approaching the façade at an angle of incidence creates on the windward side next to the inlet a low-pressure zone, whereas the pressure on the leeward side either exceeds or at least equals the value of pressure in undisturbed flow. The results for the front façade seem to indicate that an identical duct installed in the close vicinity would not be adversely affected. This would therefore enable the installation of a number of ducts with turbines in a row. There might be an overall drop in pressure on the front façade, but it would be an effect of the ensemble.

If we look at the corresponding situation at the outlet on the flat roof, the entrainment of the jet into the vortex flow along the wall/roof edge has a different impact for different angles of incidence. There is no clear relation between the angle of incidence where maximal wind speed is induced and the differential pressure to windward and leeward of the duct outlet. This might be the result of different swirl characteristics of the entraining flows.

If the wind approaches normal to the façade, no configuration shows any significant loss of suction at the flat roof edge, and the negative pressure remains uniform around the outlet. With rising angles of incidence the ducts induce a drop in suction downstream on the leeward side and a rise in suction on the windward side of the outlet. However, the minimum downstream suction is still of similar magnitude to that created by wind normal to the façade. At very large angles of incidence the situation reverses and the suction downstream exceeds the suction to windward. The angle of incidence where this transition takes place depends perhaps on the size of the duct or the strength of the jet entrainment. In order to get a clear picture of the flow situation for several ducts, it would be necessary to test combinations of ducts at various spacings.

The measured wind speed ratio along the centreline at the duct outlet is taken as a rough approximation in order to predict the performance of a module (in the fourth section) using one-dimensional streamline theory for the wind turbine. At this stage it is only possible to estimate flow rates and to get a rough assessment of the likely performance.

## Computational Fluid Dynamics (CFD) Modelling

### Modelling Approach

With the software package PHOENICS 2.2.1,<sup>9</sup> a three-dimensional analysis for the wind flow over a building block with integrated duct has been carried out. The flow domain was 1.20 m in height, 2.0 m downstream and 1.0 m upstream, and 60 cm to each side, corresponding to conditions in the working section of the wind tunnel. Because of the limited number of cells, a geometrically simple duct configuration had to be specified and the experimental model with the 90° duct was modelled without spoiler (Figure 7). For the same reason it was not possible to model the smooth bell-mouth-shaped inlet. The total number of cells,  $N_X \times N_Y \times N_Z = 20 \times 291 \times 32$ , was close to the limits of the available computational systems.

The grid requirements to model such a building with integrated duct are demanding. In order to achieve good resolution in the region of the duct, a special technique links body-fitted grid subdomains of different cell sizes and different cell numbers together (Figure 17). The alteration in the body-fitted co-ordinate direction at the subdomain connection at the duct bend has been overcome by using a non-natural linkage method. This method provides a link between two subdomains, which have geometrically a common boundary, but their co-ordinate systems are not aligned to each other. In this method of assembling highly non-orthogonal subdomains and linkage via common boundaries, the decoupling of pressure and momentum does not take place with a common staggered grid. The alternative method is the collocated velocity method.

The simulation is steady state. The wind flow is only normal to the front façade, as the three-dimensional simulation makes use of the symmetry plane as mirror plane. The flow is modelled as incompressible.

Combining the conservation equation for a fluid element with the Navier–Stokes equations, a general transport equation for a transported flow property  $\phi$  is found as<sup>6</sup>

$$\rho \frac{D\phi}{Dt} = \frac{\partial(\rho\phi)}{\partial t} + \text{div}(\rho\phi\vec{u}) = \text{div}(\Gamma \text{grad } \phi) + S_\phi \quad (1)$$

It states that the rate of increase of  $\phi$  for the fluid element plus the net rate of flow of  $\phi$  out of the fluid element due to convection is equal to the rate of increase of  $\phi$  due to diffusion and sources  $S$ . The coefficient of diffusion is  $\Gamma$ .

The implementation of the standard  $k-\varepsilon$  model makes it possible to predict the swirl pattern. It has a wide range of applicability,<sup>13,14</sup> though its limitations in cases of strong streamline curvature are well documented

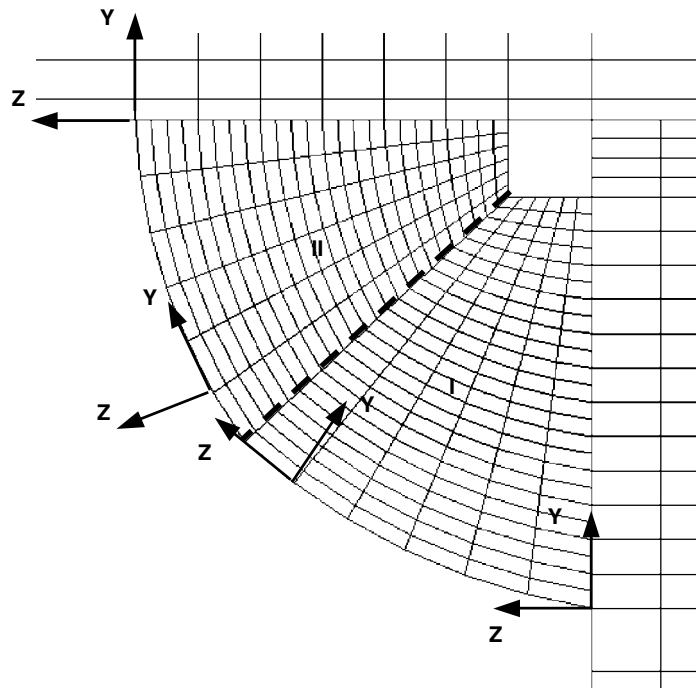


Figure 17. Gridding and subdomains for flow simulation in 90° duct

and predictions of recirculating and reattaching flows should be viewed with some caution. However, different variations are widely used to model wind flow in the built environment, and for the present study it was retained in preference to other models which are perhaps more accurate but are also more demanding of computational resources.

The default discretization scheme used in PHOENICS 2.2.1 is the hybrid differencing scheme, and SIMPLEST is the default algorithm for the iterative solution.<sup>9</sup> The inflow velocity corresponds to the average wind speed at which the wind tunnel tests were conducted ( $v = 16.5 \text{ m s}^{-1}$ ). The scalar variable of the turbulence model,  $k$ , carries as inflow condition 1% average wind tunnel turbulence intensity,<sup>15</sup> and  $\varepsilon$  is calculated based on the hydraulic diameter of the duct.<sup>14</sup> The air density corresponds to the average value as measured in the wind tunnel ( $\rho = 1.1623 \text{ kg m}^{-3}$ ). The constant kinematic viscosity was taken as  $\nu = 1.4553 \times 10^{-5} \text{ m}^2 \text{ s}^{-1}$ .<sup>16</sup>

#### *Modelled Results: the Flow through the Duct and around the Leading Roof Edge*

Very important for our purpose is the flow acceleration through the duct, which is influenced by the acceleration in the flow field around the leading edge. Above the roof the flow speeds up by around 10%–15% compared with the undisturbed flow speed at building roof height.

The flow field in the duct (Figure 18) shows evidence of separation towards the inlet. Further downstream the velocity profile recovers and the flow speeds up around the bend. The entrainment at the outlet into the surrounding flow field is influenced by the separation of the external flow at the leading edge of the building. Immediately between leading edge and duct outlet there is a region of decelerated flow in the wake of the separation at the edge.

Comparing the measured and simulated profiles of the wind speed ratio in the duct (Figures 19 and 20), there is good agreement. One has to remember that the model duct in the wind tunnel was equipped with a smoothly curved inlet (see Figure 7). This is the reason for the smaller recirculation zone at the bottom of the duct compared with the simulation, and explains the deviation of the values in the lower 20% of the duct

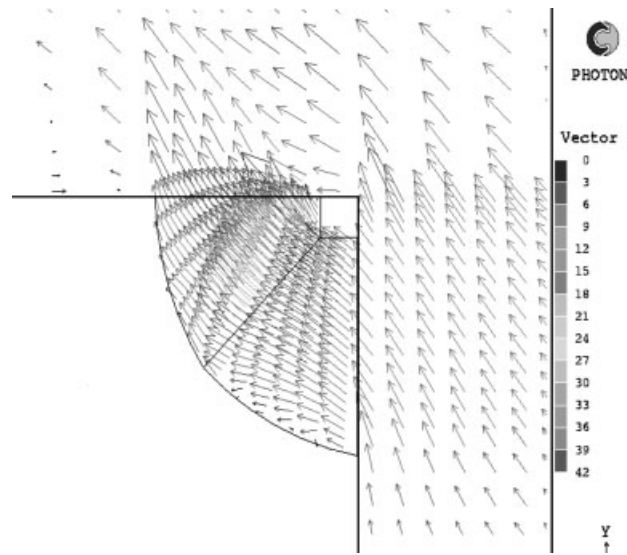


Figure 18. Duct flow, plane of symmetry

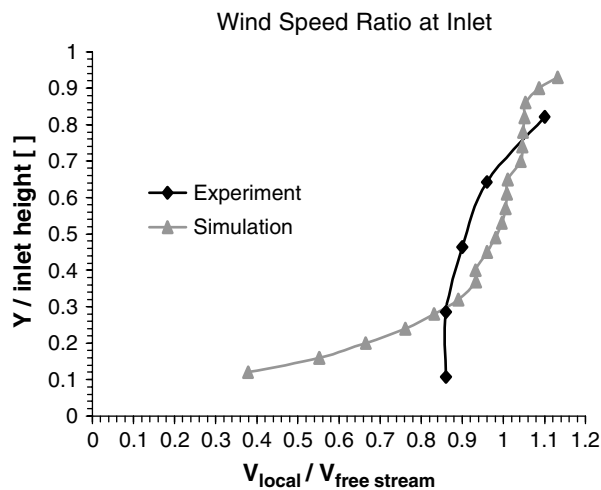


Figure 19. Vertical profile in duct inlet, at plane of symmetry

(Figure 19). Because of the limited number of cells, it was not possible to model exactly the inflow of the experimental case.

Both profiles in Figure 19 show accelerated flow towards the upper region of the duct and values of similar magnitude. A pressure drop measured at the bottom wall of the duct accompanies the simulated flow separation at the inlet (Figure 20).

The experimental values suggest a smoother inflow. Halfway through the duct the simulated and measured pressure values are about the same. In a curved duct it is generally difficult to estimate the flow field from the pressure field on the wall, as the flow might deflect into the tapping.

At the outlet, simulation and experiment predict about a maximum 15% wind speed increase, but the loss of momentum in the upwind region of the outlet seems to be more severe than as modelled (Figure 21). However, overall there is sound agreement, and very good agreement over the downwind part of the outlet.

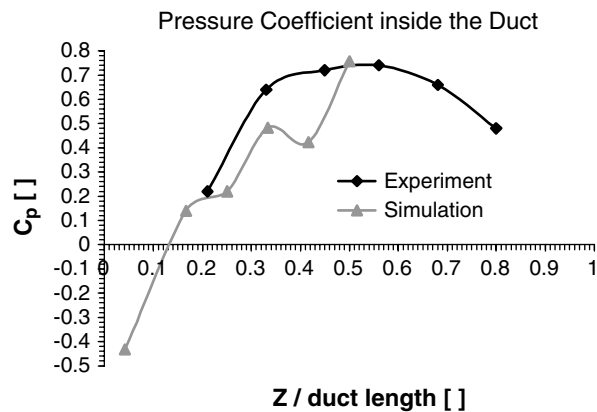


Figure 20. Pressure at the bottom wall of the duct, plane of symmetry

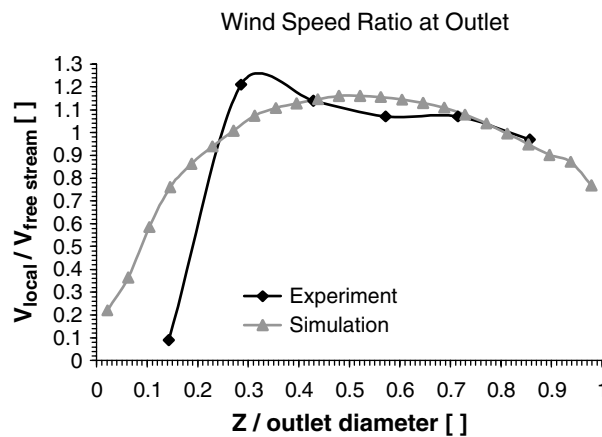


Figure 21. Velocity profile in the outlet opening, plane of symmetry

### Summary of the CFD Results and Conclusions

The simulated internal flow field through the building integrated duct agrees well with the experimental measurements. It seems that the flow inside the duct is accelerated by around 15% in this case. A smoothly curved inlet to the duct is very important to avoid flow separation.

The duct flow entrains into the separated flow beyond the roof edge and joins the mainstream over the roof without reattaching. There is no evidence that the interaction of the duct flow with the surrounding flow might restrict the induced speed or mass flow through the duct. The pressure boundary conditions of the duct flow are quite complex, in particular as the zones of inflow and outflow are not really isolated. However, the positive pressure on the front façade and the suction on the roof did not decline owing to the duct flow.

Certainly a significant amount of kinetic energy is dissipated in turbulence, both inside and outside the duct. However, it can be concluded that a well-designed duct might induce air speeds at the outlet up to 20% higher than the undisturbed freestream velocity at roof height for wind approaching normal to the façade. Clearly a spoiler over the inlet may be beneficial to guide the upflow into the inlet and widen the zone of flow separation at the leading edge over the roof, thus increasing the suction.<sup>8</sup> This was in fact confirmed in the experiments described in the second section.

According to basic fluid dynamics (Bernoulli equation), the duct induces speeds which correspond to the average pressure difference in the wider flow field between the communicating zones. For example, for stagnation pressure at the duct entrance on the front façade and a suction over the roof corresponding to

$C_p = -0.5$  (see experimental values in Figures 10 and 11), the induced speed would be around 22% higher ( $V = V_{\text{ref}}(\Delta C_p)^{1/2}$ ). Without taking energy dissipation in the duct into account, the induced wind speed is overestimated compared with the findings of this simulation and of the experiment, as might be expected.

The accuracy and versatility of the CFD modelling process were severely compromised by available computational resources. CFD clearly has much to offer here, but more detailed system models must be implemented. Rapid advances in the quality of both hardware and software are already making this more feasible.

## **Power and Energy Prediction**

### *The Prediction Model*

Building-integrated ducted wind turbine modules are still at an experimental stage. Therefore the power output characteristics are uncertain. Nevertheless, in this section an attempt is made to generate a sound model based on the data available at this stage. The characteristic of the ducted device,  $c_p(v)$ , was modelled using data from the free-standing prototype in 1994.<sup>3</sup>

As the power output is related to the free wind speed, each configuration is characterized with a parametric set of power curves according to the angle of incidence (see Figures 23 and 24).

The model incorporates two types of regulating schemes: first, the power coefficient  $c_p$  is kept constant for higher wind speeds, once it reaches its maximum; second, the resulting power is restricted to a rated value, as in pitch-regulated machines.

In order to represent a possible installation in the west of Scotland, two turbines (30° and 90° ducts with spoilers) are modelled, facing west. The predicted performance is compared with two different competitive forms of renewable energy generation for small scale application in the built environment: the free standing wind turbine type Rutland WG 910 'Standard' from the British Manufacturer Marlec Engineering Co., and the crystalline silicon solar panel type 585 'Saturn' from BP Solar.

From the model climate data file the power output values are calculated on an hourly averaged basis. The energy yield is the summation of the hourly energy production over the specific period of time.

### *The Model Climate Data File*

The prediction is based on a standard hourly climate data file for Glasgow, which has been generated from many data sets in a statistical manner and is used in the building energy simulation package ESP\_r of the Energy Systems Research Unit at the University of Strathclyde.<sup>17</sup>

The 'typical' annual wind speed roughly follows a Weibull distribution (Figure 22). Most of the time the wind is at low or medium speed. Therefore it is important to deploy a turbine with relatively good starting characteristics. However, low wind speeds contribute relatively little to the energy yield.

The prevailing wind directions are north-east and south to west, corresponding to the geographical location of Glasgow near the west coast of Scotland. North-easterly winds from Scandinavia occur mainly during the winter season. Average wind speeds are around 40% lower in summer, but incident solar energy is almost 10 times higher than in winter, which is typical for the northern latitude of Scotland. As modelled, the optimal angle for a solar panel on a Glasgow site would be around 36° from the horizontal.

### *Predicted Power Curves*

Power output from the ducted wind turbine is influenced by the possibility (in favourable conditions) of inducing high velocities in the duct. Where ducting is employed to enhance the flow, it is found (see e.g. Reference 18) that the power coefficient rises in proportion to the mass flow rate. The power characteristics shown in Figures 23 and 24 were obtained using the standard equation, increasing the values of power coefficient in proportion to the mean wind speed ratios displayed in Figure 16. This process therefore incorporates directional sensitivity effects as well.

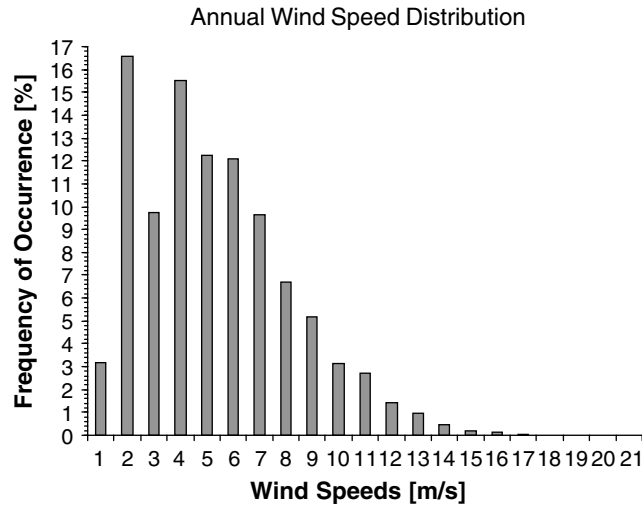


Figure 22. Annual wind speed distribution of climate model file

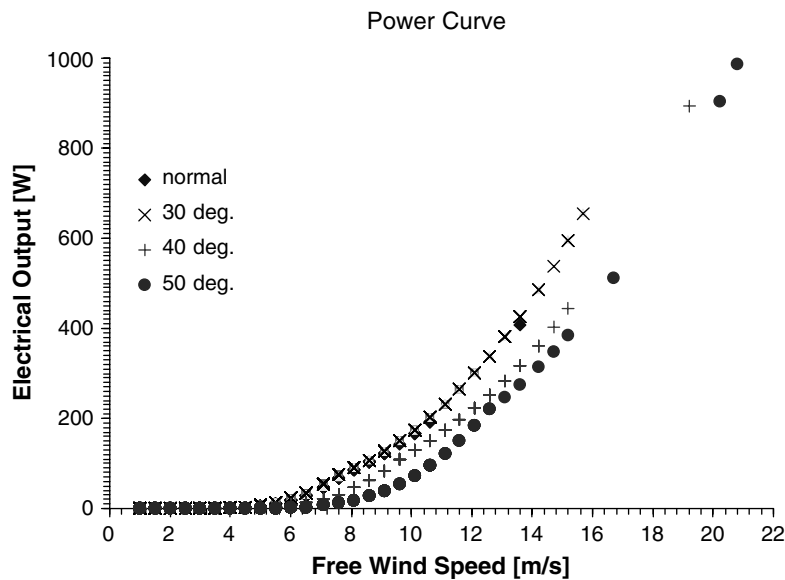


Figure 23. Modelled power curve for configuration with 30° duct and spoiler, parametric set for various angles of incidence

**Energy Yield Prediction**

The modelled hourly averaged power outputs (Figures 23 and 24) of the two configurations are the basis for estimating the monthly energy yield. In particular, the impact of different rated power values (1000, 500, 250 and 100 W) was investigated.

The monthly energy yield for the conventional wind turbine was calculated on the basis of the power curve from the manufacturer. This turbine has a smaller rotor diameter of 0.91 m, compared to the suggested ducted rotor of 1 m diameter. The photovoltaic (PV) performance was modelled with the regenerative energy simulation program MERIT, which was recently developed in the Energy Systems Research Unit at the University of Strathclyde.<sup>19</sup> In order to allow comparison, the area of the photovoltaic panel was scaled up to match the swept area of the ducted rotor.

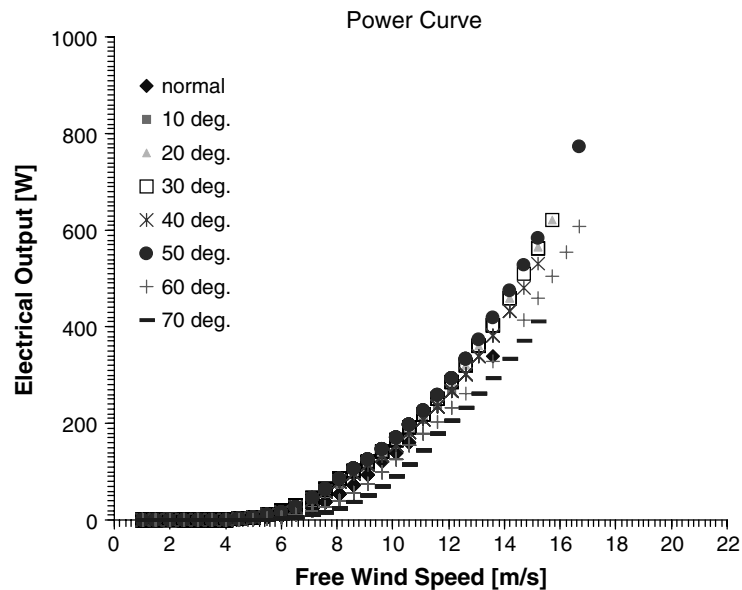


Figure 24. Modelled power curve for configuration with  $90^\circ$  duct and spoiler, parametric set for various angles of incidence

Even in the summer months (apart from July) the conventional wind turbine with its small rotor swept area and low power coefficient, which is characteristic for such a small machine, compares favourably with the PV panel (Figure 25). Its predicted annual energy yield is around twice the solar PV production (Figure 26).

Estimations of energy yield for the ducted wind turbine depend on the rated power restriction applied in the model. As the high wind speeds contribute disproportionately to the generated power, modelling of different ratings is most significantly reflected in the energy yield for the windy months. A realistic power rating may be around 250 W, which is suitable for higher wind speeds. For this rating the ducted wind turbine facing west compares favourably with the conventional turbine (Figure 25).

Figure 26 shows the impact of the rated power cut-off on the annual energy yield. A power cut-off at 500 W reduces the energy yield only marginally, and for 250 W power cut-off the annual energy yield drops by less than 10%. A significant decrease of 30%–35% in energy production is predicted for a rating of 100 W.

Generally a better performance is predicted for a device with  $90^\circ$  duct owing to the wider range of tolerated wind directions. The annual energy production of one ducted wind turbine facing west and rated at 250 W is predicted to exceed the yield from the conventional lower rated turbine. The power augmentation of the ducted wind turbine due to induced higher wind speeds in the duct compensates for the loss due to unfavourable wind directions. Hence, in order to harvest the augmented power in the wind, a higher rated generator than for the conventional turbine should be deployed.

### Discussion and Conclusions from the Power and Energy Prediction

In the presented model the predicted power and energy yield for the ducted wind turbine are significantly higher than for the conventional turbine or the photovoltaic panel. A contributory reason for the advantageous performance of the ducted wind turbine in this model may be the assumptions made in calculating the power output. A more accurate model requires information which will only become available when the ducted wind turbine is integrated in a building at full scale and tested. The presented power prediction should be interpreted with common sense as a potential.

The directional performance is modelled according to the wind tunnel experiments. So far, no work has been done to confirm these results either at large scale or through computational fluid dynamics. The

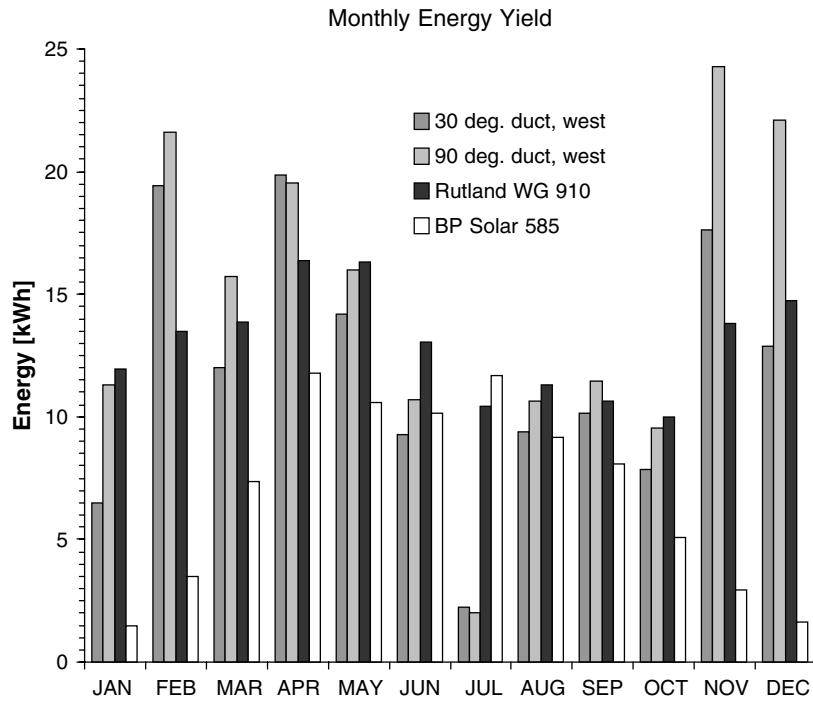


Figure 25. Monthly energy yield, 250 W power cut-off

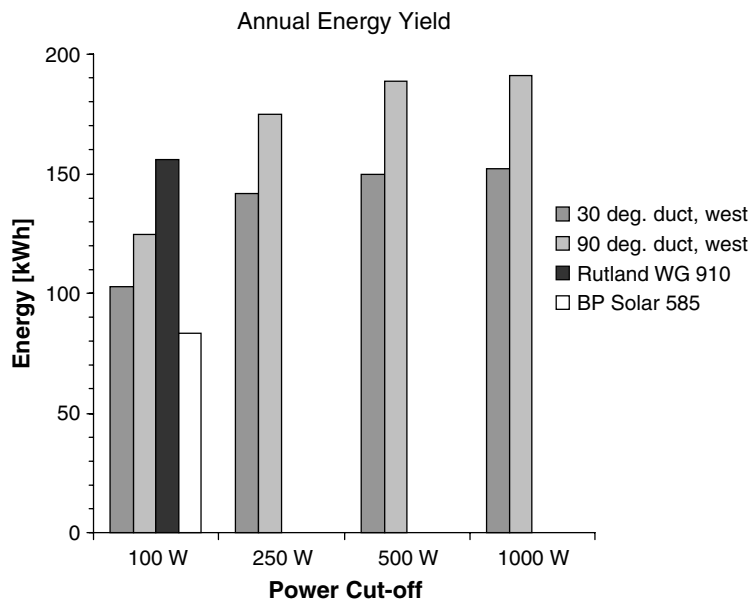


Figure 26. Annual energy yield at different ratings

directional performance is one of the most important contributions to power augmentation and to the energy yield.

The presented power prediction model may overestimate the actual power generation, but it describes other features of the turbine well. For example, the turbine will have a parametric band of power curves according

to its directional sensitivity. Also, the energy yield in certain cases will be significantly higher than for a conventional small turbine.

### **General Discussion and Conclusions**

Experimental measurements on a model building with an integrated duct were carried out in a low-speed wind tunnel. There is evidence that, for some combinations of duct and spoiler, air speeds more than 30% above the velocity of the approaching freestream are induced in the duct. Also, the duct tolerates a large angle of incident wind, in some cases as much as  $\pm 60^\circ$ . At larger angles of incidence the increased suction over the roof due to vortex development seems to play an important role. The induced wind speed in the duct appears to peak at a non-zero angle of incidence.

There is a discrepancy between the pressure coefficient standards on a flat roof at full scale<sup>12</sup> and for small-scale wind tunnel models.<sup>11</sup> For full scale a much higher suction is observed at the leading roof edge than at model scale. Therefore it might well be that a full-scale prototype would perform better than predicted by model tests. On the other hand, full-scale turbulence generated in the surrounding built environment could have an adverse effect on the flow through the duct. Field trials at realistic scale are the only way to resolve this issue.

Of particular interest is the assessment of the impact of the duct flow entrainment into the suction zone over the roof. As a high suction is accompanied by recirculating flow, disturbance of this pattern might cause significant changes in the pressure. The pressure distribution upwind and downwind of the jet entrainment was measured, but no clear pattern emerged, with different combinations of duct and spoiler leading to contrary results. However, even in the worst case the suction on the roof still approximated to the value measured for inflow normal to the façade. Thus there is evidence that the installation of several turbines in a row along the wall/roof edge is feasible, but a future detailed investigation of multiple ducts is necessary for a final evaluation.

The correspondence between experimental and simulated results of the duct flow is encouraging, but the results have limitations for performance estimation and power output prediction. Limitations in the complexity of the CFD model made it impossible to incorporate a resistance in the duct to represent the effect of a turbine. Likewise, the wind tunnel experiments were performed on an unobstructed duct. The velocities observed allowed the relative performance of geometrical adjustments to be assessed, but accurate predictions of potential power output require a more sophisticated approach. The presented power prediction model, based on one-dimensional streamline theory, therefore only illustrates the potential of such a device. It predicts a rather higher monthly energy yield than for other competitive deployments of renewable energy generation in the built environment.

It is clearly necessary to develop a more representative computational model in terms of grid refinement, turbulence modelling and simulation of the effects of the turbine. Reliable CFD predictions would accelerate optimization of the geometry of the system, which is still at an early stage.

### **Acknowledgements**

The authors would like to thank Dipl-Ing Matthias Leyk and all other former students, technicians and colleagues at the Department who contributed to the presented work. It was carried out within the Marie Curie Research Fellowship, Commission of the European Communities, DG XII, Directorate-General for Science, Research and Development, under the 4th framework, JOULE—Non Nuclear Energy Research; Project: Wind Energy in the Built Environment, Project No. JOR3-CT97-5008 (DG12-DEMA).

### **References**

1. Webster GW. Devices for utilizing the power of the wind. US Patent 4154556, 1979.
2. Nasr el-Din S, Grant AD, Lee CK. A wind energy module for low power applications. In *Proceedings of the International Conference on Energy for Rural and Island Communities VI*, Twidell J (ed.). Pergamon: Oxford, 1992.

3. Grant AD, Nasr el-Din SA, Kilpatrick J. Development of a ducted wind energy converter. *Wind Engineering* 1994; **18**: 297–304.
4. Dannecker R, Quinonez Varela G, Grant A. Development of the building integrated ducted wind turbine module. *Proceedings of the 21st British Wind Energy Association Conference (BWEA21)*, Cambridge, September 1999; 141–147.
5. Grant AD, Dannecker R. A hybrid PV/wind energy module for integration in buildings. *Proceedings of the 16th European Photovoltaic Solar Energy Conference and Exhibition*, Glasgow, May 2000; 2033–2036.
6. RE-Start (Renewable Energy Strategies and Technologies for Regenerating Towns); Targeted Project under the RUE (Rational Use of Energy) in the Building Sector; THERMIE Programme, 4th Framework. Commission of the European Communities, DG XVII, Directorate-General for Energy and Transport: Brussels, 1996.
7. Dannecker RK, Grant AD. Wind energy in the built environment. *Final Scientific Report, Project No. JOR3-CT97-5008 (DG12-DEMA)*, submitted to the Commission of the European Communities, DG XII, Directorate-General for Science, Research and Development, JOULE—Non Nuclear Energy Research, 1999.
8. Dannecker RKW. Wind energy in the built environment: an experimental and numerical investigation of a building integrated ducted wind turbine module. *PhD Thesis*, University of Strathclyde, Glasgow, 2001.
9. Spalding DB. *Phoenix Encyclopaedia (Version 2.1)*. CHAM (Concentration, Heat and Momentum Ltd): London, 1994.
10. Leyk M. Aerodynamical investigation of a ducted wind turbine. *Externe Studienarbeit*, Fachgebiet Energietechnik und Reaktoranlagen, Fakultät für Maschinenbau, Technische Universität Darmstadt/Student Research Project, Energy Systems Division, Department of Mechanical Engineering, University of Strathclyde, Glasgow, 1997.
11. ESDU Engineering Science Data Unit). *Wind Engineering—Mean Loads on Structures*, Vol. 2b: Fluid Forces, Pressures and Moments on Rectangular Blocks; Item No. 71016. ESDU International: London, 1993.
12. The assessment of wind loads. Part 6: Loading coefficients for typical buildings. *BRE Digest 346*, British Department of the Environment, Building Research Establishment Garston, 1989.
13. Launder BE, Spalding DB. The numerical computation of turbulent flows. *Computer Methods in Applied Mechanics and Engineering* 1974; **3**: 269–289.
14. Versteeg HK, Malalasekera W. *An Introduction to Computational Fluid Dynamics—the Finite Volume Method*. Wiley: New York, 1995.
15. ESDU (Engineering Science Data Unit). *Wind Engineering—Wind Speed and Turbulence, Vol. 1a: Characteristics of Atmospheric Turbulence near the Ground, Part II: Single Point Data for Strong Winds (Neutral Atmosphere); Item No. 85020*. ESDU International: London, 1985; (with amendments A to F, 1993).
16. Franzini JB, Finnemore EJ. *Fluid Mechanics with Engineering Applications* (9th edn). McGraw-Hill: New York, 1997.
17. Clarke JA. *Energy Simulation in Building Design*. Adam Hilger: Bristol, 1985.
18. Hansen MOL, Sorensen NL, Flay RGF. Effect of placing a diffuser around a wind turbine. *Wind Energy* 2000; **3**: 207–213.
19. Born FJ. Aiding renewable energy integration through complementary demand–supply matching. *PhD Thesis*, University of Strathclyde, Glasgow, 2001.